RESEARCH PAPER

Comparative in vitro toxicity assessment of spiked anisotropic gold nanostructures

Bankuru Navyatha · Seema Nara

Abstract Gold nanobipyramids and nanostars are the nanostructures with sharp protrusions which endow them with unique electromagnetic and photochemical properties making them useful in various imaging and photoablation therapy applications of different diseases especially cancer. For any in vivo applications, it is desirable to understand the comparative cytotoxic profile of these nanostructures. Studies comparing the cytotoxicity of differently spiked nanostructures with each other are relatively scarce. In this context, the current study focuses on the investigation of biocompatibility and cytotoxicity of nanobipyramids and nanostars on RBCs and PC3 prostate cancer cell line respectively. The synthesized nanostructures are thoroughly characterized using UV-Vis spectroscopy, transmission electron microscopy (TEM), energy-dispersive X-ray spectroscopy (EDX), and inductively coupled plasma mass spectroscopy (ICP-MS) analysis. Cytotoxicity studies are accomplished using metabolic assays (MTT and neutral red assays) and analyzing the membrane integrity of treated cells using flow cytometry. The results show nanostars to be less cytotoxic and more biocompatible than nanobipyramids. This study holds high significance for using the spiked nanostructures in in vivo applications.

Keywords Nanobipyramids · Nanostars · Biocompatibility · Cytotoxicity · Membrane integrity · Hemolysis

B. Navyatha · S. Nara (✉)
Department of Biotechnology, Motilal Nehru National Institute of Technology, Allahabad, UP 211004, India
e-mail: seemanara@mnnit.ac.in

e-mail: seemanara@gmail.com

Introduction

Anisotropic gold nanostructures are evolving as cutting edge in various fields like biosensing, catalysis (Silveira et al. 2019), imaging/spectroscopy (Quaresma et al. 2014; Oliveira et al. 2019), therapeutics, and theranostics (Feng et al. 2017). The asymmetric growth of anisotropic nanostructures in different directions leads to the formation of sharp branches/protrusions over their surface. These branches possess a high surface to volume ratio compared with their core/base which enhances their capacity to absorb light. This property of intense light absorption helps in increasing the resolution of imaging modalities, endowment of therapeutic properties by amplifying surrounding tissue temperature (photothermal therapy), and/or release of reactive oxygen species (photodynamic therapy) (Yuan et al. 2012; Feng et al. 2017). Recently, gold nanoparticles (GNPs) of sizes 1.9 nm and 15 nm have achieved better attention as contrast agents in imaging and these have been approved by the FDA which have been marketed with a trade name AuroVist (Domey et al. 2015; McQuaid et al. 2016). Profound research has been carried out on various anisotropic gold nanostructures

like nanorods, nanocages, and nanoshells for their applications in nanomedicine which have demonstrated to be better contrast agents in imaging and ablation therapy (An et al. 2017; Navyatha and Nara 2019). These fascinating properties of anisotropic nanostructures depend not only on the size of nanostructures but also on their shape. Among all anisotropic nanostructures, gold nanobipyramids (GNBs) and gold nanostars (GNSs) are gaining much attention due to their sharp edges and surface protrusions respectively. These sharp tips endow the cellular uptake of nanostructures due to the decline in the contact angle with the cell (Duan and Li 2013). Their sharp tips have very high surface plasmon resonance properties as compared with the core or blunt ends (nanorods) which confer increased bioimaging and photothermal abilities to these nanostructures (Yuan et al. 2012; Tian et al. 2015; Bibikova et al. 2017).

However, for in vivo applications, toxicity of nanostructures is a critical issue and a burning debate in the field of nanomedicine (Fratoddi et al. 2015; Jia et al. 2017). Toxicity imposed by nanostructures is multifactorial (Sharma et al. 2012) and depends on the nanostructures' physicochemical properties, such as size, shape (Wang et al. 2013; Wozniak et al. 2017; Steckiewicz et al. 2019), surface charge, concentration, surface functionalization (Alkilany et al. 2009; Deng et al. 2017), nature of the cell (such as type of the cell, state, metabolic status) (Steckiewicz et al. 2019), environmental conditions (such as medium composition, relative humidity, presence or absence of cell growth specific compounds) (Li and Riviere 2016; Kokkinopoulou et al. 2017), nature of the targeting molecules, and route of administration (Zhang et al. 2010). The shape of the nanostructures is crucial as it determines their cellular uptake efficiency (Wang et al. 2013) and fate upon internalization. Hence, the shape could be a determinant in deciding the toxicity of nanostructures. Comparative studies on the cytotoxicity of gold nanostars, nanorods, and nanospheres are there, but there is relative dearth of literature on the cytotoxicity of nanobipyramids. Considering the aforementioned significance of spiked anisotropic nanostructures in bioimaging and therapeutic applications, it is justified to do a comparative study on their toxicity before any in vivo application. In this context, the present study is undertaken to investigate the cytotoxicity of two differently shaped anisotropic nanostructures—bipyramids and stars with varying degrees of pointed spikes. PEGylation is a well-known strategy to make the nanostructures biocompatible (Ahmad et al. 2018); hence, PEGylated nanostars and nanobipyramids are used for determining their toxicity on PC3 prostate cancer cell line.

Materials and methods

Materials

All reagents and chemicals used are of analytical grade or HPLC grade. All reagents and chemicals used for cell culture are of cell culture grade. Gold (III) chloride hydrate, sodium borohydride ($NaBH_4$), cetyl trimethyl ammonium chloride (CTAC) solution, DCFDA dye, polyethylene glycol methyl ether thiol (mPEG-SH) are purchased from Sigma-Aldrich, USA. Cetyl trimethyl ammonium bromide (CTAB), silver nitrate ($AgNO_3$), 8-hydroxyquinoline (HQ), neutral red dye, Triton X-100, bovine serum albumin, sodium hydroxide (NaOH) are purchased from Sisco Research Laboratories Pvt. Ltd., India. Ascorbic acid is purchased from Global Chemie, India. RPMI-1640, fetal bovine serum, trypsin, propidium iodide (PI) dye, 3-(4,5-dimethylthiazol-2-yl)-2,5-diphenyl tetrazolium bromide (MTT) reagent are purchased from HiMedia Laboratories Pvt. Ltd., India. The cell line used in the study is procured from the National Centre for Cell Science, Pune, India. Fresh human blood samples are collected from healthy volunteers within the Department of Biotechnology, MNNIT, Allahabad, with their due consent.

Synthesis of nanostructures

Nanostructure synthesis is performed using a two-step seed-mediated approach. The synthesis scheme for both nanostructures is summarized as a flow chart in Supplementary information (Fig. S1) and detailed ahead.

Synthesis of gold nanobipyramids

The synthesis of GNBs is performed as previously reported with some modification (Chateau et al. 2015). This seed-mediated method uses low potential reducing agent 8-hydroxyquinoline for the growth of GNBs. Briefly this two-step method involves seed synthesis and growth of seed.

Synthesis of seed solution

To 4 ml of 95-mM CTAC solution, 4 ml of 0.5-mM $HAuCl_4$ solution is added and kept at 20 °C under stirring for 20–30 s. To this, 72 µl of 250-mM HNO_3 (nitric acid) is added and kept under vigorous stirring at 1000 rpm for 20–30 s. Now, 100 µl of freshly prepared, ice-cold reducing solution (mixture of 50-mM $NaBH_4$ and 50-mM NaOH) is added and stirring is continued for 1 more minute. Finally, 16 µl of 1 M trisodium citrate is added. The flask is removed from stirring and kept in a water bath pre-heated at 80–85 °C for 60 min.

Synthesis of the growth solution

Firstly, the surfactant mixture of 6-mM CTAB and 140-mM CTAC is prepared. To a clean flask, 4 ml of this surfactant mixture and 40 µl of 25-mM $HAuCl_4$ are added and gently stirred for 20–30 s. To this, 12 µl of 10-mM $AgNO_3$ is added and stirring is continued for another 20–30 s. Now, 40 µl of 0.4-M HQ is added and stirred at 420 rpm for 1 min. Finally, 40 µl of as-prepared seed solution is added and kept in a water bath at 40–45 °C for 15 min. After 15 min, 30 µl of HQ is added to the flask and kept in a water bath again for 90 min at the same temperature. The gold nanobipyramids are harvested by washing this solution twice in Milli-Q water for 10 min at 8000 rpm. The final pellet is used for PEGylation as detailed ahead.

Synthesis of gold nanostars

Gold nanostars are synthesized as per the surfactantless, seed-mediated method reported elsewhere with slight modification (Yuan et al. 2012). Briefly, the method includes synthesis of seed and growth of gold nanostars.

Synthesis of seed solution

To 100 ml of boiling $HAuCl_4$ (1 mM) solution, 15 ml of 1% trisodium citrate solution is added and kept under stirring for 15 min. On completion of 15 min, the solution is cooled to room temperature under stirring. The cooled seed solution is stored at 4 °C until further use.

Synthesis of the growth solution

To 10 ml of 0.25-mM $HAuCl_4$ solution, 10 µl of 1-M HCl and 100 µl above-prepared seed solution are added sequentially and stirred at 700–800 rpm for 20–30 s. To this, 100 µl of 3-mM $AgNO_3$ and 50 µl of 100-mM ascorbic acid are added within no time and stirred for another 30 s. To maintain the stability of gold nanostars under long-term storage, the as-synthesized gold nanostars are surface coated with 10% bovine serum albumin (BSA) solution (10 µl per 1 ml of gold nanostars solution) and incubated for 24 h. The BSA-coated GNSs (BSA-GNS) solution is washed twice in Milli-Q water by centrifuging for 10 min at 5000 rpm. The final pellet is used for PEGylation as detailed ahead.

Effect of buffer on surface capping of gold nanostructures with polyethylene glycol

The PEGylation of nanostructures and their stability studies are carried out in three different buffers viz sodium carbonate (2 mM, 4 mM, 6 mM, and 8 mM), Tris-borate (50 mM) buffer, and Tris-HCl (50 mM) buffers as well as in Milli-Q water for after incubation at different time intervals (2, 4, 6, 8, 24 h). To the harvested nanostructure pellet, 400 µl of respective buffer and 25 µl of 2-mM mPEG-SH solution are added and incubated at room temperature under shaking at 180 rpm for different time intervals (2–24 h). The unbound PEG is removed by spinning at 8000 rpm (for gold nanobipyramids) and 5000 rpm (for gold nanostars) for 10 min. Finally, the obtained pellet is dissolved in 0.6–1 ml of 1× phosphate buffer saline (PBS) solution, pH 7.4 to maintain the final absorbance of nanostructures ≥ 1. The solution is checked for stability by visible aggregation, comparative UV-Vis scan, and NaCl stability assay.

Characterization of gold nanostructures

The UV-Vis spectra of as-synthesized gold nanobipyramids and gold nanostars are analyzed on CARY60 UV-Vis spectrophotometer (Agilent Technology) for determining their surface plasmon peaks. Transmission electron microscopy (TEM, H-7500, Hitachi) is conducted to determine their morphology and dimensions. The hydrodynamic size of nanostructures in PBS and growing medium (RPMI-1640 with 2% fetal bovine serum) is determined

using Nanotrac-Microtrac Wave-II dynamic light scattering (DLS) instrument. The surface capping of nanostructures with PEG is confirmed by FTIR analysis using RZX (Perkin Elmer) Fourier transform infrared spectrophotometer. The elemental composition of PEGylated nanostructures is determined using FESEM combined with energy-dispersive X-ray spectroscopy (SEM-EDX) (FESEM: Su8010, Hitachi; EDS: XFLASH6130, Brukers). The concentration of elemental gold in both PEGylated nanostructures is determined using inductively coupled plasma mass spectroscopy (ICP-MS) analysis (Element XR, Thermo Fisher Scientific). As these nanostructures are synthesized and stored in water as a solvent, the aqueous sample is directly used for the above-mentioned analyzing techniques. X-ray diffraction analysis of both nanostructures is performed using the Rigaku X-ray diffractometer with Cu-Kα monochromatic source having λ of 1.54 A$^\text{o}$ at a step size of 0.025 degree. The samples are coated on silicon wafers and then processed for analysis.

Toxicity assessment of gold nanobipyramids and gold nanostars

The toxicity assessment of gold nanobipyramids and gold nanostars is determined by assessing cytotoxicity on the human prostate cancer cell line, PC3, and biocompatibility on human RBCs as explained ahead. For all studies, an equal concentration of elemental gold (as determined by ICP-MS) is used as a treatment in the range of 1–20 μg/ml. Appropriate positive controls (0.1% Triton-X100 for all MTT assays, neutral red assays, and biocompatibility assays; paraformaldehyde for PI staining; Hydrogen peroxide for DCDFA staining) and negative controls (2% RPMI-1640 culture medium) are kept in all assays.

Cytotoxicity assessment on the PC3 cell line

>This is carried out on the PC3 cell line by analyzing mitochondrial activity using MTT assay, lysosomal activity using neutral red assay, and the integrity of the plasma membrane by PI staining and its subsequent analysis through flow cytometry. ROS generation is determined by DCFDA staining and its subsequent analysis through flow cytometry.

Cell culture

Human prostate cancer cell line, PC3, from NCCS, Pune, India, is cultured in RPMI-1640 supplemented with 10% fetal bovine serum (FBS). The cells are maintained at 37 °C, 5% CO_2, humidity to achieve optimal growth. The sub-culturing is carried out by trypsinization using 0.25% (w/v) trypsin/EDTA.

Determination of mitochondrial activity

The viability of cells is determined by measuring the activity of mitochondrial dehydrogenase enzyme present in live cells using MTT dye. For performing the assay, the cells are trypsinized and seeded in a 96-well plate at a density of 10^5 cells/ml in each well and incubated for 16–18 h for promoting adherence to the surface. The culture medium is discarded; the cells are washed with PBS or incomplete culture medium and treated with different concentrations of nanobipyramids and nanostars for 1 h and 24 h at 37 °C. After completion of treatment, cells are washed with PBS or incomplete culture medium and then incubated with 100 μl of 0.5-mg/ml MTT solution for 4 h at 37 °C. The formazan crystals are dissolved by adding 150 μl of absolute DMSO followed by incubation at 37 °C for 15–20 min. Finally, the absorbance is read at 570 nm. The percentage cytotoxicity is calculated using the formula reported previously by Stolle and group (Stolle et al. 2005).

$$\%\text{Cytotoxicity} = 100 - \left[\left(\frac{\text{Absorbance of treated sample at 570 nm}}{\text{Absorbance of untreated sample at 570 nm}} \right) \times 100 \right]$$

Determination of Lysosomal activity

Lysosomal activity defines the cellular viability, and it can be measured using a neutral red dye that

accumulates in the lysosomes of healthy cells. Briefly, the trypsinized cells are seeded in a 96-well plate at a density of 10^5 cells/ml and incubated for 16–18 h. Different concentrations of gold nanostructures are added

to the cells and incubated for 1 h and 24 h at 37 °C. On completion of treatment, cells are washed with PBS or incomplete culture medium and incubated with neutral red dye solution for 2 h at 37 °C. Finally, the neutral red solution is discarded and the cells are lysed by incubating them with acidified ethanol at 37 °C for 15–20 min. The absorbance is read at 540 nm. The percentage of cytotoxicity is calculated as

$$\%\text{Cytotoxicity} = 100 - \left[\left(\frac{\text{Absorbance of treated sample at 540 nm}}{\text{Absorbance of untreated sample at 540 nm}} \right) \times 100 \right]$$

Investigation of membrane integrity

One of the ways to determine the cell viability is to examine the integrity of the cell membrane. This can be achieved by staining with various live cell impermeable dyes. One of them is propidium iodide (PI), which enters into the non-viable cells via porous plasma membrane and binds to the nucleic acids. The PI dye has the excitation of 493 nm and emission at 636 nm, when it binds to DNA/RNA the excitation/emission shifts to 535 nm/ 617 nm. This shift in wavelength differentiates the bound and unbound PI. In the current study, the membrane integrity is determined by quantifying the fluorescence intensity of PI stain via flow cytometry. For flow cytometry analysis, the cells are seeded at 10^5–10^6 cells/ml and incubated for 16–18 h at 37 °C and then treated with different concentrations of gold nanostructures for 1 h at 37 °C. The cells are washed and re-suspended in PBS to ensure the final cell density be 10^6 cells/ml. Finally, the cells are incubated with PI dye (10 μg/ml) for 20 min at 37 °C in dark and then the events/cells are acquired by the BD Accuri C6 flow cytometer.

Analysis of ROS generation

ROS-driven cell damage is one of the behind mechanisms involved in the cytotoxicity of various nanoparticles (Fard et al. 2015). To determine and quantify the generated ROS, non-fluorescent dye, DCFDA is implemented and been quantified by flow cytometry. DCFDA, a live cell permeable dye, taken up by the viable cells, deacetylated to a non-fluorescent compound by cellular esterases which in turn converted to a fluorescent compound 2,7-dichlorofluorescein by ROS via oxidation. For the measurement of ROS by DCFDA, cells are cultured and harvested as per the procedure discussed in the previous section and then incubated with the dye for 30 min in dark. Finally, the fluorescence intensity of DCFDA is measured by flow cytometry.

Cellular uptake studies on the PC3 cell line

Cellular uptake studies are carried out by quantifying the amount of nanostructures taken up by the cells using ICP-MS analysis. The cells are seeded at a density of 1×10^6 cells/ml in a 12-well plate and incubated for 24 h. After achieving the confluence of 80–85%, the cells are treated with nanobipyramids and nanostars at a concentration of 20 μg/ml and at an exposure time of 1 h and 24 h. On the completion of incubation time, the medium is discarded and cells are washed with 1× PBS. Later, the cells are etched with 1 ml of etching solution (I_2/KI solution in the ratio of 0.34 mM/2.04 mM) for 3 min and cells are washed thrice with 1× PBS. Finally, the cells are processed for ICP-MS analysis by digesting with aqua regia at 90 °C overnight to release the gold ions from the intracellular nanostructures (Li and Monteiro-Riviere 2016). The cellular uptake of nanostructures is represented in terms of percentage uptake of gold w.r.t. time calculated as per the method reported previously by Xie et al. (2017).

$$\text{Percentage uptake of gold} = \frac{\text{Total ppb of gold determined by ICP-MS analysis within the cells}}{\text{Total ppb of gold at the time of exposure with cells}} \times 100$$

Biocompatibility assessment on RBCs

The biocompatibility of nanostructures is performed on human red blood cells (RBCs). The biocompatibility is determined by calculating the percentage of hemolysis and the hematocrit value after treating RBCs with gold nanobipyramids and nanostars.

Quantification of hemolysis

The hemolysis is quantified by determining the ratio of hemoglobin released into plasma (plasma hemoglobin) to total hemoglobin (Sasidharan et al. 2016). Briefly,

fresh blood from a healthy donor is collected in EDTA vacutainer. To 1 ml of freshly drawn blood, 100 μl of various concentrations of gold nanobipyramids and gold nanostars is added and incubated for 1 h and 24 h at 37 °C. After incubation, the treated blood samples are centrifuged for 10 min at 4500 rpm. The upper plasma portion is carefully collected in a fresh tube and diluted with 0.01% sodium carbonate solution in 1:1 ratio. Finally, the absorbance is noted at 415 nm, 380 nm, and 450 nm.

The plasma hemoglobin is calculated by applying following equation.

$$\text{Plasma hemoglobin (mg/dl)} = \frac{((2 \times A_{415}) - (A_{380} + A_{450}) \times 1000 \times \text{dilution factor})}{E \times 1.655.}$$

where $E = 79.46$, which is the value of molar absorptivity of oxyhemoglobin that has maximum absorption at 450 nm; the constant value 1.655 is fractioned to minimize the interference raised due to the turbidity of plasma.

$$\%\text{Hemolysis} = \left(\frac{\text{Plasma hemoglobin of the treated sample}}{\text{Total hemoglobin of the blood}}\right) \times 100$$

Determination of percent hematocrit value

The blood collected in EDTA vacutainer from a healthy donor is incubated with different treatments of both gold nanostructures for 1 h and 24 h at 37 °C. After incubation, the treated blood sample is transferred to a Wintrobe tube and centrifuged for 10 min at 1000 rpm. Upon centrifugation, different layers are formed and the length of the RBCs is measured based on the gratings present on the tube.

The percent of hematocrit value (Hct) is calculated as follows:

$$\%\text{Hematocrit value} = \left(\frac{\text{length of the packed RBCs}}{\text{length of the whole blood}}\right) \times 100$$

Statistical analysis

All the assays are repeated three times in duplicate each time and then the mean ± standard deviation is calculated. The statistical difference between the different

groups is determined by applying one-way ANOVA analysis by Prism 5 software. The difference is indicated as p value, and $p < 0.05$ is considered to be statistically significant.

Results

Synthesis of gold nanobipyramids

The gold nanobipyramids are synthesized using the seed-mediated method. The seed solution turns pale reddish orange upon the addition of $NaBH_4$, the reducing agent. The crystallinity of the seeds is enhanced due to the combined effect of high temperature (85 °C for 1 h) and CTAC. Using CTAC instead of CTAB produces chloride ion that has less affinity to Au atoms as compared with the bromide ion and therefore results in the formation of polycrystalline seeds (Chateau et al. 2015). Such polycrystalline seeds lead to the formation of sharp-edged nanobipyramids in contrast to nanorods (formed due to monocrystalline seeds produced by the usage of CTAB). The synthesis of seed is highly sensitive and it depends on various parameters like the temperature at which the reaction has conducted and the reactants as well as the rate of addition of sodium borohydride, the purity of the components, and the pH of the solution. The synthesis of seeds is the most fragile step and highly irreproducible, and also, the quality of

seed dictates the quality and homogeneity of nanobipyramids.

During the growth step, the use of the dual surfactant (CTAB/CTAC) has played a major role due to the difference in the affinity of chloride ion and bromide ion with gold. Due to the high affinity of bromide ions on Au{100} face, the growth of this face is slowed which may lead to the formation of the nanorods. Chloride ions from CTAC prevent nanorod formation and accelerate the growth on this facet, thereby forming sharp edges. Further, use of low potential reducing agent 8-hydroxyquinoline produces gold ions at a slow rate which permits the deposition of gold ions on the Au{110} leading to the formation of a broad base at the center compared with the edges (Chateau et al. 2015; Nikoobakht and El-Sayed 2003). Silver ions play a key role by complexing with bromide ion which in turn forms a complex with gold ions to initiate the growth of nanobipyramids and hence the presence of bromide ion in the form of CTAB is essential for the initiation of 1D nanostructures' growth.

Synthesis of gold nanostars

The synthesis of gold nanostars is achieved by applying a surfactantless seed-mediated method. The seed solution is synthesized by reducing gold salt with trisodium citrate. In the growth step, addition of hydrochloric acid before the addition of ascorbic acid reduces its reduction potential leading to the formation of sharp and high number of protrusions. Silver nitrate and ascorbic acid need to be added simultaneously to regulate the nanostar formation. If silver nitrate is added prior to ascorbic acid, silver chloride precipitates out due to the reaction of silver ions with chloride ions in gold chloride solution. In contrast, if silver nitrate addition is delayed, nanosphere formation takes place owing to the reduction of gold chloride by ascorbic acid. So the silver nitrate and ascorbic acid are added in no time (Yuan et al. 2012). The surface coating with BSA has increased the stability of the nanostars.

Effect of buffer on surface capping of gold nanostructures with polyethylene glycol

On PEGylation in different buffers, it is seen that both nanostructures have aggregated within no time in Tris-HCl and Tris-borate as well as in Milli-Q water irrespective of the time of incubation. However, both gold nanostructures are most stable in 2-mM sodium carbonate buffer compared with 4-mM, 6-mM, 8-mM concentrations (Fig. S2a-d, Supplementary information) as evidence by the reduction of intensity at λ_{max} in high buffer concentrations. The stability is maximum at 24 h of incubation with PEG-SH in 2-mM sodium carbonate buffer. This swift aggregation with other buffers might be due to the rapid displacement of CTAB/CTAC bilayer in the case of nanobipyramids and BSA layer over the nanostars (Fig. S3a-b) leading to a sudden drop in repulsive forces between the individual nanostructures. But sodium carbonate buffer might provide an environment for steady-state replacement of surface layer with PEG molecules which endows their stability (Zhang and Lin 2014). So, for further cytotoxicity analysis, PEGylation of both the nanostructures is carried out in 2-mM sodium carbonate buffer and stored in 1× PBS. To confirm whether the stability of nanostructures is due to PEG molecules or surfactant molecules, the surfaced capped nanostructures are treated with 3.4-M sodium chloride. PEGylated nanostructures did not show any aggregation, whereas the aggregation is observed with naive nanostructures.

Characterization of nanobipyramids and nanostars

The UV-Vis spectra of the as-synthesized gold nanobipyramids showed TSPR at a wavelength of 555 nm, LSPR at a wavelength of 845 nm (Fig. 1a) and TEM micrographs have proven that most of the particles are of bipyramidal shape possessing an average length of 67.81 nm with a width of 24.95 nm (Fig. 1b).

Similarly, gold nanostars characterized by UV-Vis spectroscopy (Fig. 1c) are displaying a broad peak between 750 and 850 nm. TEM micrographs (Fig. 1d) also show that the synthesized nanostructures possess sharp protrusions and most of them are of the same shape. Size distribution of PEGylated nanobipyramids (Fig. S4, Supplementary information) and nanostars (Fig. S5, Supplementary information) in PBS does not vary much from when they are suspended in growth medium for 1 h and 24 h. This indicates that both nanostructures are stable in growing medium used in the study even after 24 h.

FTIR analysis is carried out to confirm the PEGylation of both gold nanostructures. For nanostar synthesis, no detergent such as CTAB is used; rather, BSA is used for surface stabilization followed by PEGylation. The FTIR spectra of only BSA, BSA-
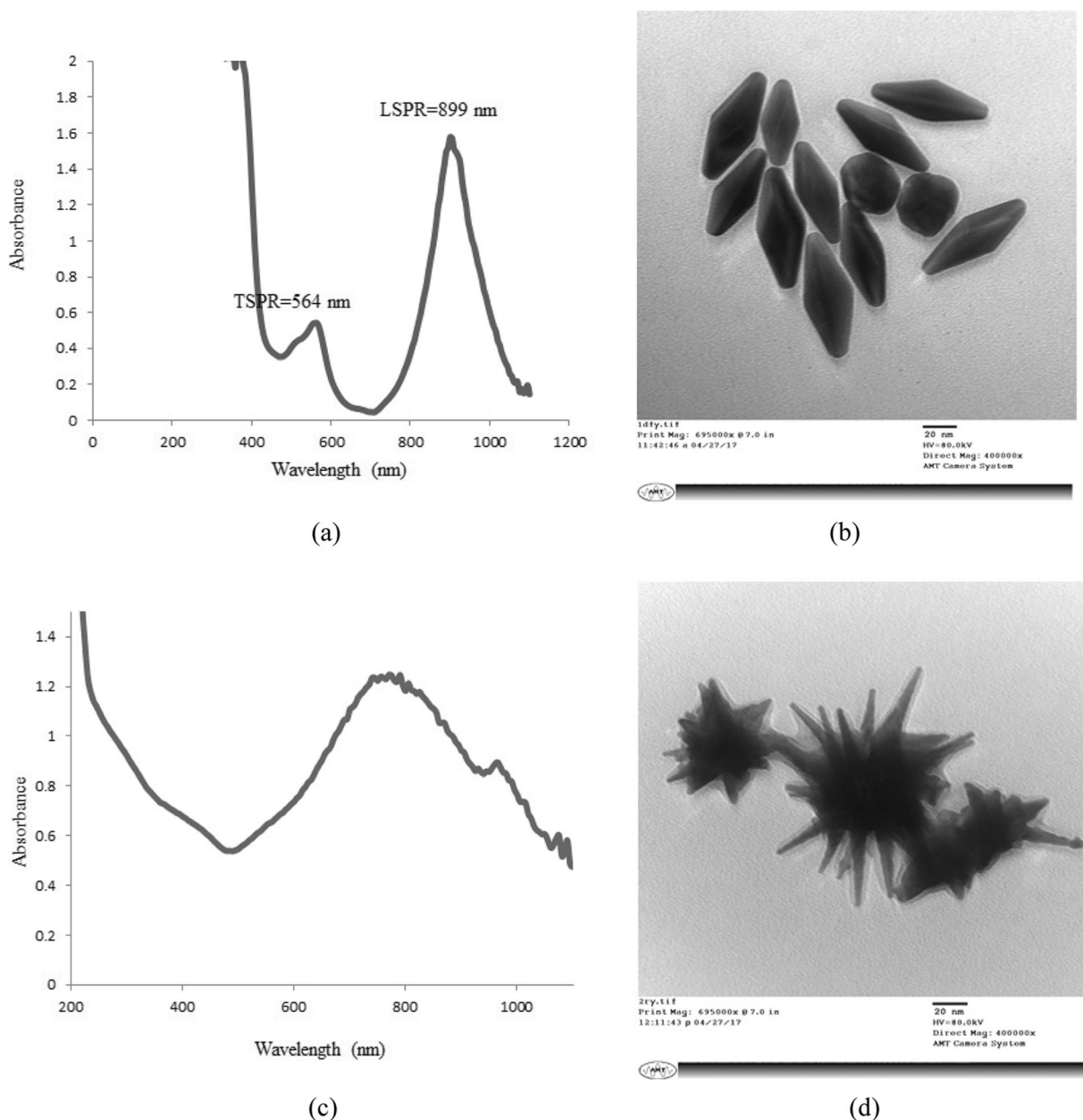
(a)

(b)

(c)

(d)

Fig. 1 UV-Vis spectrum of **a** GNBs and **c** GNSs. TEM micrograph of **b** GNBs and **d** GNSs

stabilized nanostars, only mPEG-SH, and PEGylated nanostars are represented in Fig. S6b (Supplementary information). The characteristic peaks at 685 cm^{-1} and 2569 cm^{-1} in mPEG-SH molecules are due to thioethers (C–S stretch) and thiol (S–H stretch) respectively. Presence of these peaks in PEGylated GNSs confirms their surface functionalization with PEG. The peak at 1660 cm^{-1} in PEGylated GNSs is due to an amine group which could be attributed to BSA on their surface.

During the synthesis of nanobipyramids, CTAB is used as a stabilizer which is gradually replaced with PEG by repeated centrifugation. The FTIR spectra of only CTAB, CTAB-stabilized nanobipyramids, only mPEG-SH, and PEGylated nanobipyramids are depicted in Fig. S6a (Supplementary information). The FTIR spectra of only CTAB do not depict any characteristic peak which could be used to confirm the removal of CTAB from PEGylated GNBs. The prominent peaks
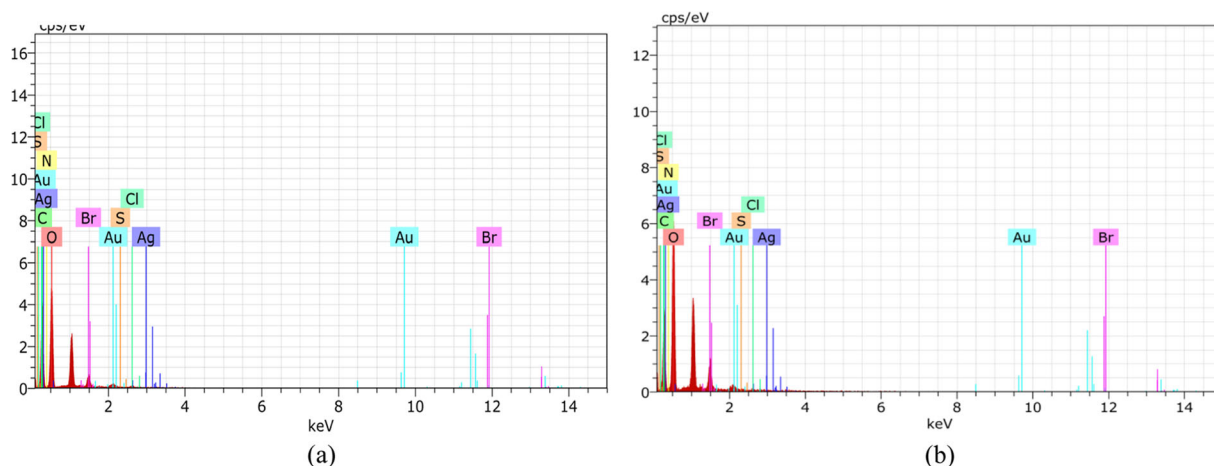
Fig. 2 EDX spectrum of **a** PEGylated GNBs and **b** PEGylated GNSs

in only CTAB (3266 cm^{-1} and 1637 cm^{-1}) are also observed in mPEG-SH. The peak at 3266 cm^{-1} is attributed to O–H stretch. The peak at 1637 cm^{-1} is attributed to C–N stretch (CTAB) as well as C–C stretch (mPEG-SH), and therefore, this peak appears in both these molecules. Instead in the FTIR spectra of mPEG-SH only, the characteristic peaks at 687 cm^{-1} and 2584 cm^{-1} are observed which corresponds to thioethers (C–S stretch) and thiol (S–H stretch). Presence of these peaks in PEGylated GNBs confirms the introduction of PEG on their surface. PEGylated GNBs also depicts a prominent peak at 1340 cm^{-1} which corresponds to O–H bending.

Elemental composition of PEGylated nanostructures is done using EDX spectroscopy. Figure 2a and b depict the EDX spectrum of PEGylated nanobipyramids and PEGylated nanostars respectively. The significant peak of gold in the EDX spectrum strongly confirmed the presence of a gold element in nanobipyramids and nanostars. The presence of sulfur, carbon, and oxygen peaks relate to the thiol-terminated PEG which is capped over the surface of gold nanostructures.

Figure 3 depicts the XRD pattern of nanobipyramids and nanostars. The XRD pattern in both the nanostructures shows peaks at 38° and 62° which corresponds to (111) and (220) planes of face-centered cubic of gold. This confirms that both the nanostructures are synthesized in single phase and the sharpness of the peaks indicates the crystallinity of nanostructures. The peaks at 69° and 70° attribute to the silicon wafer used for the analysis of nanostructures (Evcimen et al. 2015).

The ICP-MS analysis of both nanostructures determined the concentration of elemental gold in nanobipyramids and nanostars as 37.526 ppm and 43.615 ppm, respectively. These concentrations are used for further cytotoxicity and biocompatibility studies by converting them into micrograms per milliliter.

Cytotoxicity assessment of PEGylated nanobipyramids and nanostars

Determination of mitochondrial activity

Mitochondrial activity is directly related to the activity of cellular metabolism, and so determining their metabolism is much more helpful for calculating the toxicity of various compounds. MTT assay is widely used in in vitro cytotoxicity assay in which tetrazolium dye is reduced by the
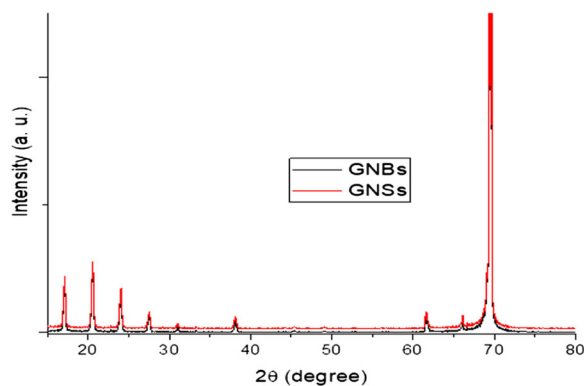

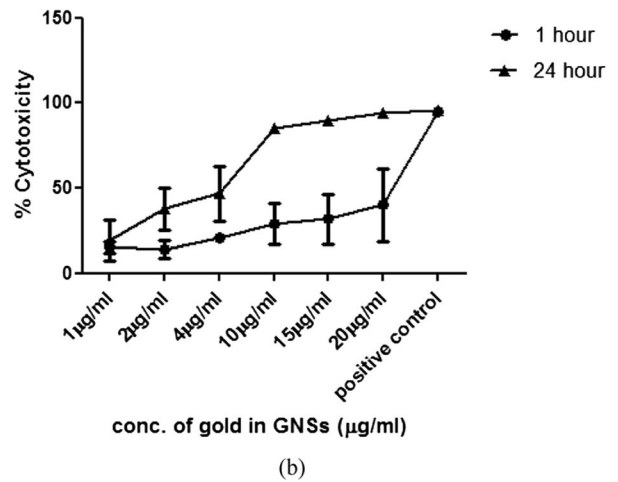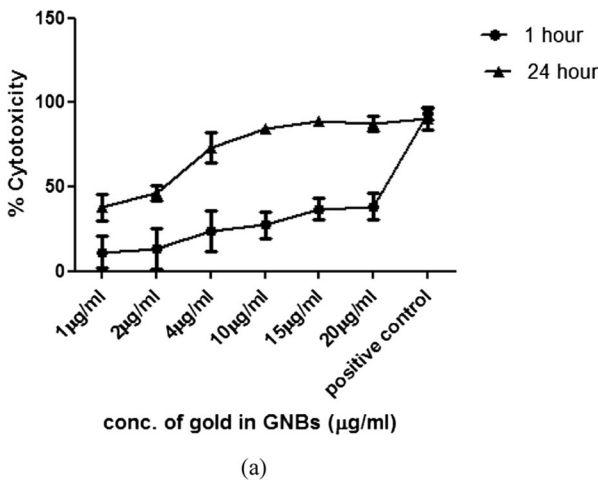**Fig. 3** XRD pattern of GNBs and GNSs

(a)

(b)

Fig. 4 Toxicity profiling of GNBs and GNSs on PC3 cell line assessed using MTT assay. **a** Percentage cytotoxicity of GNBs is 47% and 93% at the highest test concentration after 1 h and 24 h

respectively. **b** Percentage cytotoxicity of GNSs is 37% and 87% at the highest test concentration after 1 h and 24 h respectively

mitochondrial dehydrogenases to formazan crystals which can be spectrophotometrically read at 570 nm. Figure 4a and b show the percentage cytotoxicity of gold nanobipyramids and gold nanostars respectively on the basis of MTT assay data. The toxicity of both nanostructures has elevated with an increase in their concentration and the exposure time. Gold nanobipyramids showed the toxicity in the range of ~3–47% after 1 h of exposure whereas the toxicity has drastically elevated to 93% at the highest concentration (20 μg/ml) after 24 h of treatment. Similarly, gold nanostars showed the toxicity of 37% and 87% at their highest concentration of 20 μg/ml after 1 h and 24 h of treatment.

Determination of Lysosomal activity

The activity of the lysosomes is determined by their ability to accumulate the neutral red dye, a supravital dye. Figure 5a and b show the percentage cytotoxicity of gold nanobipyramids and gold nanostars respectively. The % toxicity observed for nanobipyramids and gold nanostars at the highest test concentration is observed to be 32% and 20% respectively at 1 h whereas it is 91% and 83% respectively at 24 h of exposure time.

The results of both MTT assay and neutral red assay for both the nanostructures are statistically significant with a p value < 0.0001.
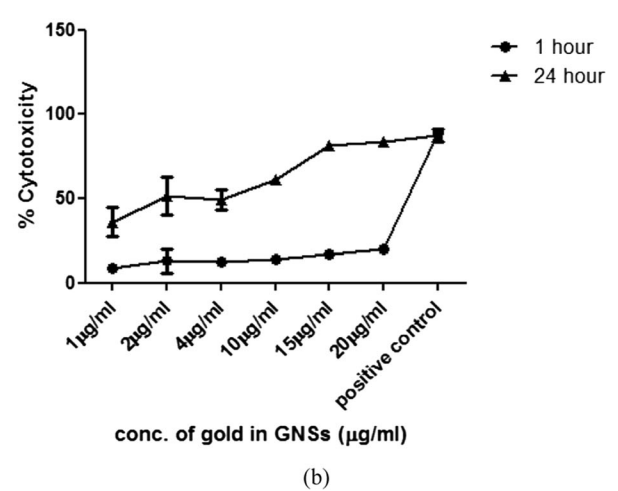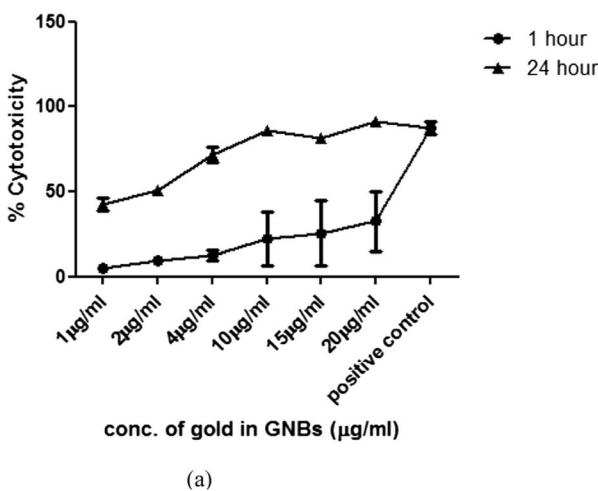

(a)

(b)

Fig. 5 Toxicity profiling of GNBs and GNSs on PC3 cell line assessed using neutral red assay. **a** Percentage cytotoxicity of GNBs is 32% and 91% at the highest test concentration after 1 h

and 24 h respectively. **b** Percentage cytotoxicity of GNSs is 20% and 83% at the highest test concentration after 1 h and 24 h respectively

Investigation of membrane integrity using PI staining

PI is a dead cell staining dye, and the fluorescence exhibited by the cells can be correlated to the number of dead cells. The gating strategy of the cells and positive controls for PI and DCFDA staining is depicted in Supplementary information (Fig. S7 and Fig. S8 respectively). Figure 6a and b represent the mean fluorescence of PI exhibited by the cells after treatment with gold nanobipyramids.

The data shows that nanobipyramids are very toxic at the highest concentration (20 μg/ml). Figure 6c and d show the mean fluorescence intensity of nanostars at various concentrations. The mean fluorescence intensity of nanobipyramids is ~4.5 times more than that of nanostars at the highest treatment concentration (20 μg/ml). This indicates greater cell damage by nanobipyramids, and the results seem consistent with that of MTT and neutral red assays.
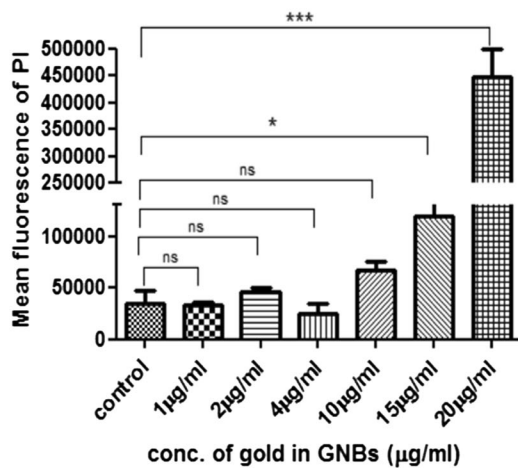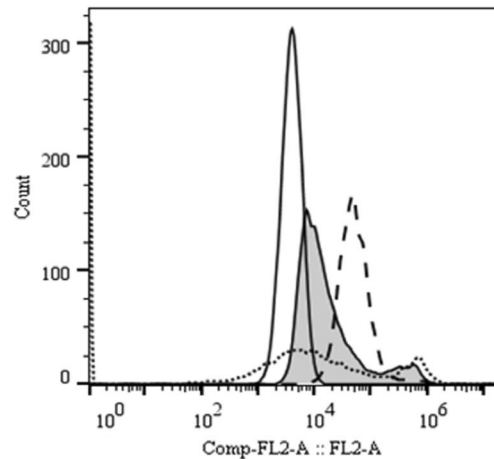
(a)
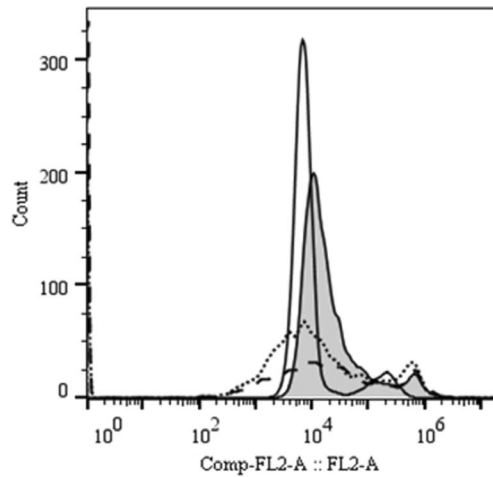
(b)
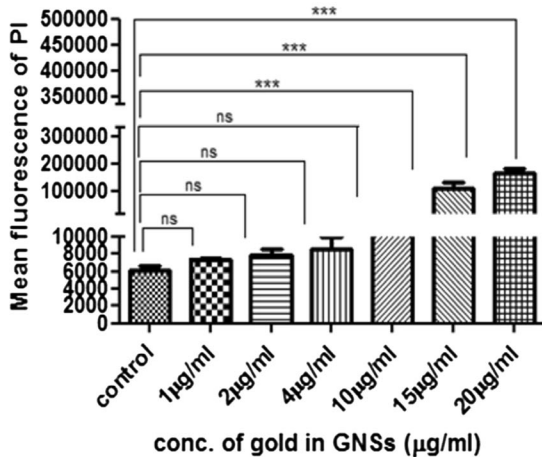
(c)

(d)

Fig. 6 a Histogram depicting the mean fluorescence of PI exhibited by PC3 cell line treated with PEGylated GNBs and their b overlaid histogram depicting the increase in fluorescence of PI, c overlaid histogram depicting the increase in fluorescence of PI exhibited by PC3 cell line treated with PEGylated GNSs, and their d overlaid histogram depicting the increase in fluorescence of PI.

Number sign for a and c: statistical analysis compared with control represents the p value, P = ns (non-significant), P = *** (< 0.0001), P = ns (non-significant). Double number sign for b and d (solid line: unstained negative control; shaded line: stained negative control; dotted line: 1 μg/ml of nanostructures; dashed line: 10 μg/ml of nanostructures)
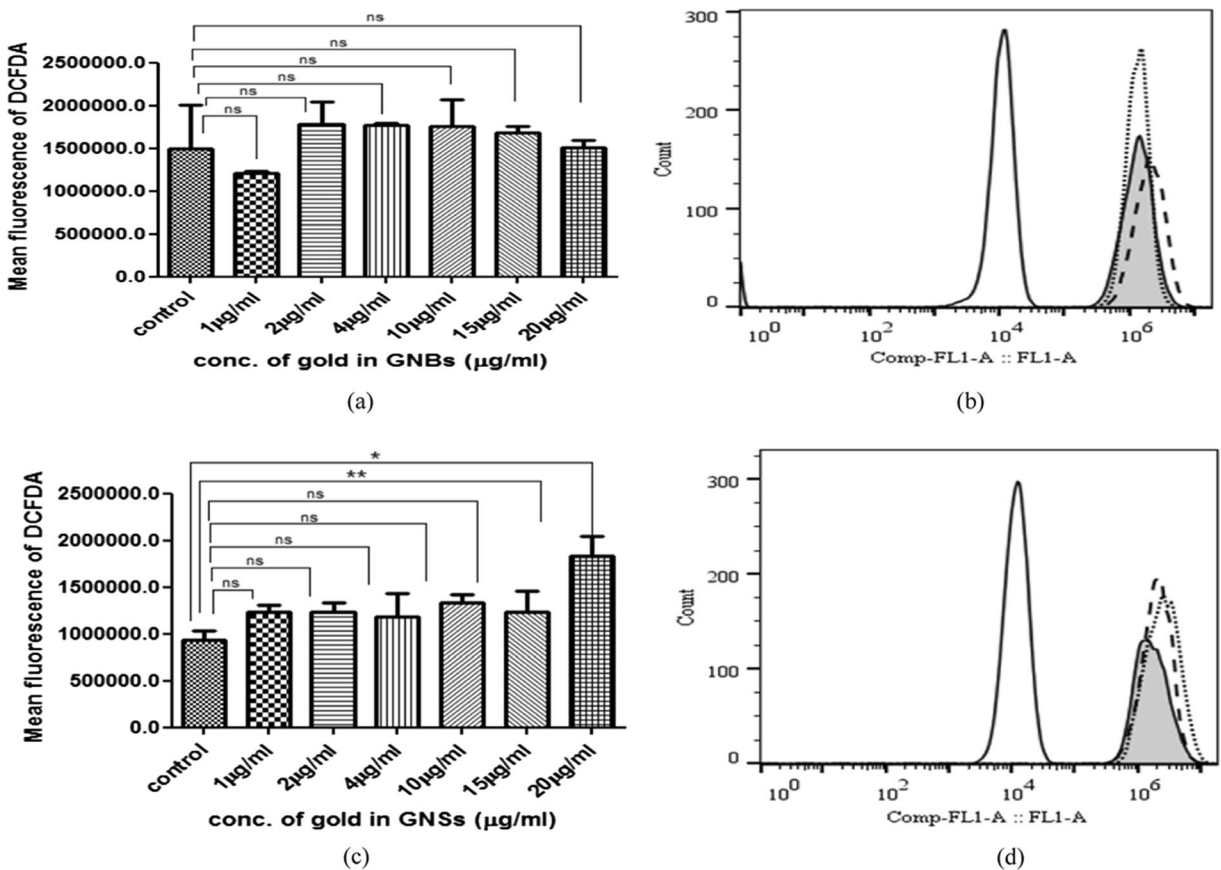
(a)

(b)

(c)

(d)

Fig. 7 Histogram depicting the mean fluorescence of DCFDA exhibited by nanostructures treated PC3 cell line. **a** PEGylated GNBs. **c** PEGylated GNSs. The statistical analysis compared with control represents the *p* value, P = ns (nonsignificant), P = ** (< 0.001), P = * (< 0.01). Overlaid histogram depicting the increase in fluorescence of DCFDA exhibiting by nanostructures treated PC3 cell line. **b** PEGylated GNBs. **d** PEGylated GNSs (solid line: unstained negative control; shaded line: stained negative control; dotted line: 1 μg/ml of nanostructures; dashed line: 10 μg/ml of nanostructures)

Analysis of ROS generation by DCFDA

The cells generate ROS in optimal amounts during cellular functions. When the ROS generation exceeds the optimal amount, they damage the cells either by apoptosis or necrosis. The percentage conversion of DCFDA into fluorescein dye by ROS can be related to the concentration of ROS generated within the cell. Based on this principle, the ROS generated within the cells induced by nanostructures is determined. Figure 7 shows the mean fluorescence generated by the cells treated with gold nanobipyramids and nanostars. ROS generation seems to be constant with changing concentrations of both nanostructures. Moreover, this change is not very significant as compared with negative controls. Hence, it could be concluded that none of these nanostructures is significantly generating reactive oxygen species and ROS is not responsible for their toxicity.

Cellular uptake studies on the PC3 cell line

The cellular uptake studies are carried out at 1 h and 24 h exposure with the highest test concentration, i.e.,
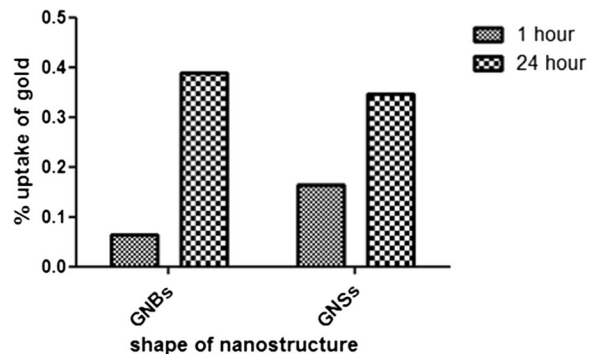

Fig. 8 Histogram showing the percent uptake of gold by PC3 cell line after 1-h and 24-h exposure with nanobipyramids and nanostars at a concentration (20 μg/ml)
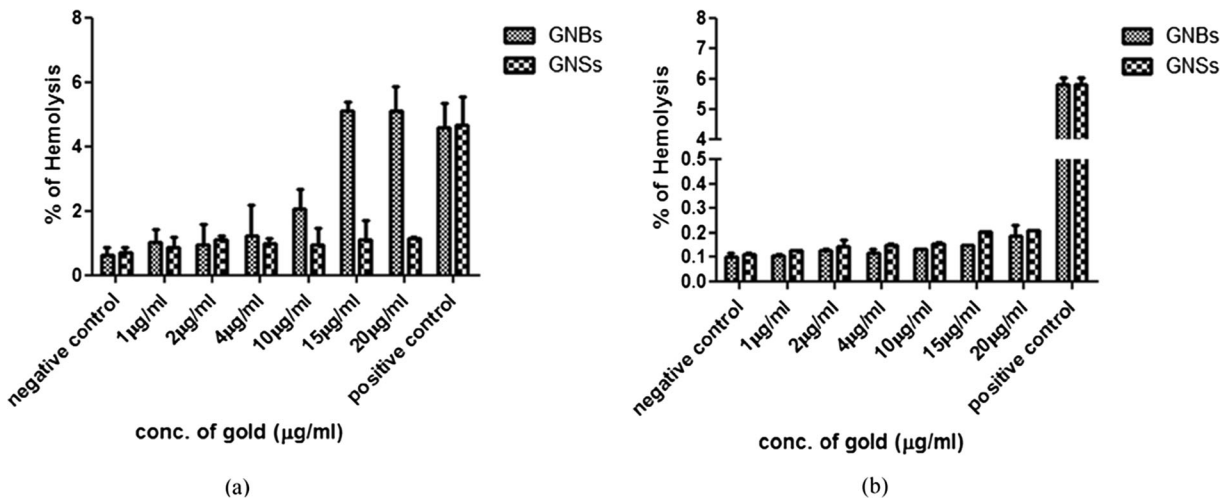
(a)

(b)

Fig. 9 Hemolytic profiling of nanostructures at different times of exposure. **a** Percentage hemolysis at 1-h exposure with PEGylated GNBs and PEGylated GNSs is 5% and 1.16% respectively at the highest concentration (20 μg/ml) w.r.t. negative control (0.6%). **b**

Percentage hemolysis at 24-h exposure with PEGylated GNBs and PEGylated GNSs is 0.19% and 0.2% respectively at the highest concentration (20 μg/ml) w.r.t. negative control (0.1%)

20 μg/ml of nanostructures. The percentage of intracellular elemental gold as quantified by ICP-MS shows a time-dependent increase irrespective of the shape of the nanostructure (Fig. 8). At 1-h exposure, the percent intracellular gold for nanobipyramid and nanostar treatments is calculated to be 0.0631% and 0.1654% respectively. This intracellular gold at 24-h exposure has increased to 0.3892% and 0.347% for nanobipyramids and nanostars respectively.

Biocompatibility analysis of PEGylated nanobipyramids and nanostars

Quantification of percentage hemolysis

The percentage of hemolysis is quantified by estimating the hemoglobin released from the lysed RBCs into plasma at 380 nm, 415 nm, and 450 nm after the treatment of freshly drawn blood
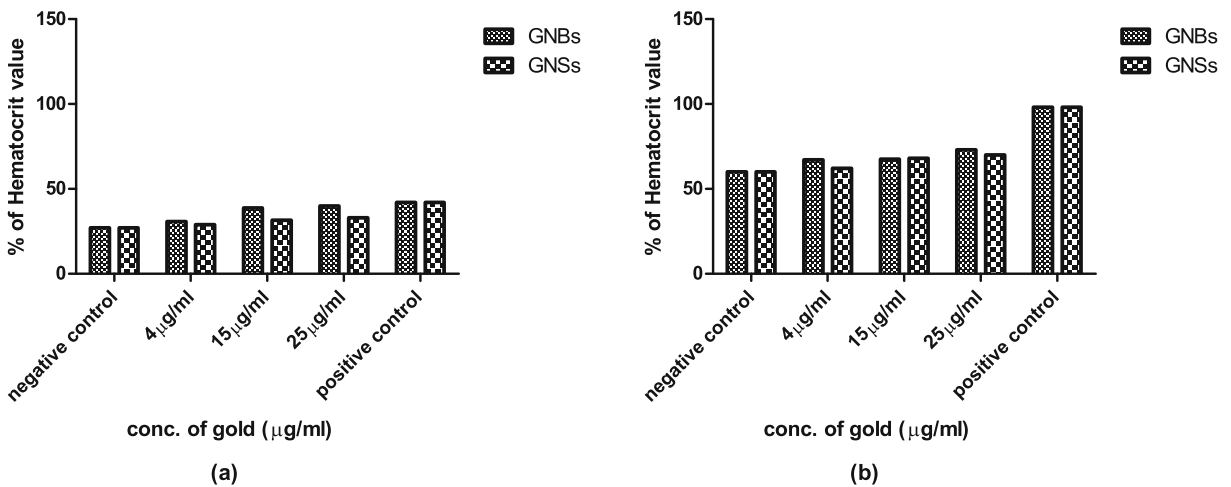

(a)

(b)

Fig. 10 Hematocrit profiling of nanostructures at different times of exposure. **a** %Hct at 1-h exposure with PEGylated GNBs and PEGylated GNSs is 5% and 1.16% respectively at the highest concentration (25 μg/ml) w.r.t. negative control (0.6%). **b** %Hct

at 24-h exposure with PEGylated GNBs and PEGylated GNSs is 0.19% and 0.2% respectively at the highest concentration (20 μg/ml) w.r.t. negative control (0.1%)

Table 1 Comparative analysis of percentage cytotoxicity of nanostructures at the highest concentration (20 μg/ml) assessed by MTT assay and neutral red assay with % cellular uptake at 1-h and 24-h exposure time

Shape of nanostructure	% cytotoxicity (MTT assay) 1-h exposure	% cytotoxicity (NR assay)	% cellular uptake	% cytotoxicity (MTT assay) 24-h exposure	% cytotoxicity (NR assay)	% cellular uptake
Nanobipyramids	47	32	0.063	93	91	0.389
Nanostars	37	20	0.165	87	83	0.347

with different concentrations of gold nanostructures. Figure 9a and b show the hemolytic profile of gold nanobipyramids and gold nanostars respectively at different times of exposure. The data show that nanobipyramids cause increased hemolysis of RBCs at higher concentrations (15 and 20 μg/ml) only. On the contrary, it is seen that nanostars are more biocompatible as there is no significant change in percentage hemolysis of RBCs as compared with the negative control. The one-way ANOVA analysis also confirmed that the data for both nanostructures is significant ($p < 0.0001$). These results are also in accordance with ASTM (American Standards for Testing and Materials) reference which says that percentage hemolysis > 5 after balancing the values of negative control are considered as hemolytic.

Measurement of hematocrit value

The %Hct value is calculated using the packed cell volume method. Figure 10a and b represent %Hct values of nanobipyramids and nanostars respectively. At 1-h exposure, %Hct values of nanobipyramids and nanostars are 41% and 32% respectively at the highest treatment whereas the %Hct value of negative control is 28%. With the increase in the exposure time of nanostructures to 24 h, the %Hct value of nanobipyramids and nanostars as well as negative control has increased to 73%, 70%, and 60% respectively at the same treatment concentration. This indicates that in our study, %Hct value holds more significance at 1-h exposure time because at 24-h exposure the negative control values are themselves very high. One-hour %Hct values show PEGylated nanostars to be relatively more biocompatible to normal blood cells than nanobipyramids.

Discussion

The in vivo application of nanostructures mainly depends on their cytotoxicity which in turn relies on multiple factors such as size, shape, and physicochemical properties of nanostructures. In this context, the current study has focused on the comparative cytotoxicity profiling of gold nanobipyramids and nanostars on the PC3 cell line. For the stable synthesis of nanobipyramids, cationic surfactant CTAB is employed whereas nanostars are synthesized using a surfactantless method. Since CTAB is well reported to attribute toxicity to the nanostructures, we have modulated the surface of synthesized nanostructures with PEG (Alkilany et al. 2009; Alkilany et al. 2012; Wang et al. 2016). These PEGylated nanobipyramids and nanostars are used for their toxicity assessment so that any difference in the toxicity could be correlated to their shape.

Cytotoxicity studies are carried out using MTT and neutral red assay and correlated with cellular uptake of elemental gold by ICP-MS. The results of both cytotoxicity assays are in good agreement with each other. Both tests demonstrated a gradual increase in the toxicity of both nanostructures in a concentration-dependent manner at 1 h and 24 h exposure time. Further, it is observed that the toxicity of both nanostructures is ~ 2.5 times higher at 24-h exposure as compared with 1-h exposure. However, the toxicity of nanostars at both exposure times is slightly lesser than nanobipyramids at any particular concentration. ICP-MS data also establishes a higher cellular uptake at 24-h exposure time. However, it is observed in ICP-MS data that percent uptake of nanostars is more than nanobipyramids at initial 1-h exposure which becomes approximately equivalent after 24 h. Careful correlation of ICP-MS data with toxicity data reveals that at short exposure time (1 h), internalization of nanostars is more yet their toxicity is less than that of nanobipyramids (Table 1), whereas at longer exposure time (24 h), the toxicity and percent

uptake of nanostars is relatively less than those of nanobipyramids. Thus, it indicates that high cellular uptake does not always induce high cytotoxicity which is in accordance with the recent report (Lee et al. 2019). As indicated above, the differential cellular uptake and toxicity of two nanostructures are more evident at brief exposure which could be attributed to the different shapes of the nanostructures. Further, we have determined the IC50 value of both nanostructures taking into account the 24-h exposure data of MTT assay as per NIH guidelines on in vitro cytotoxicity (NIH Publication No. 01-4499 2001) which says MTT assay to be more valid for calculating IC50 value. IC50 values for nanobipyramids and nanostars are calculated to be 3.536 μg/ml and 4.149 μg/ml respectively.

The differential toxicity of the two nanostructures at short exposure of 1 h as discussed above is also confirmed through flow cytometry analysis. Nanobipyramids have shown a higher degree of membrane damage than nanostars. Flow cytometry analysis of ROS generation by DCFDA staining has shown insignificant ROS generation by both the nanostructures in the PC3 cell line. It indicates that the toxicity of these nanostructures is not ROS mediated. Nevertheless, nanobipyramids have shown greater membrane damage than nanostars.

The biocompatibility of nanostructures is studied on RBCs by determining percentage hemolysis and hematocrit values. The percentage hemolysis values for both nanostructures are below the said limit of American Standards for Testing and Materials. Both the nanostructures have shown biocompatibility towards RBCs at higher concentration (20 μg/ml), of which nanostars are comparatively more biocompatible (Figs. 9 and 10). These results are in line with the findings of other studies (Sasidharan et al. 2016) which demonstrate that the albumin-coated gold nanostars have shown only ~ 0.2% hemolysis at the concentration of 100 μg/ml whereas in another study nanobipyramids have shown the hemolysis of ~ 55% at a concentration of 60 μg/ml (Zhao et al. 2018).

Thus, on the basis of 1-h cytotoxicity data and IC50 (24 h), it can be said that nanobipyramids are relatively more toxic than nanostars. Though a direct comparison of cytotoxicity of bipyramids and nanostars has not been reported previously, comparative studies on the cytotoxicity of nanostars with nanospheres and nanorods are available. Our finding is in accordance with the studies of Lee et al. (2019) and Favi et al. (2015) that also reported low cytotoxicity of nanostars compared with nanospheres. Further, Wozniak et al. (2017) have reported that the cytotoxicity of nanoparticles is related to their core size. Particles with smaller core size (such as nanospheres and nanorods) are more toxic than nanostructures (nanostars, nanoflowers, nanoprisms) possessing larger core size. Both nanobipyramids and nanostars are spiked structures, but the overall hydrodynamic diameter of the former is less than that of the latter which could be one of the reasons for the lesser toxicity of nanostars. Also, the cellular uptake is not directly correlated with toxicity as mentioned before. Thus, studies are further required to unravel the mechanism of differential cytotoxicity of these nanostructures. The study could be beneficial in employing these nanostructures for any in vivo study.

Compliance with ethical standards

Conflict of interest   The authors declare that they have no conflict of interest.

References

Ahmad N, Ahmad R, Alam MA, Ahmad FJ (2018) Enhancement of oral bioavailability of doxorubicin through surface modified biodegradable polymeric nanoparticles. Chem Cent J 12: 65. https://doi.org/10.1186/s13065-018-0434-1

Alkilany AM, Nagaria PK, Hexel CR, Shaw TJ, Murphy CJ, Wyatt MD (2009) Cellular uptake and cytotoxicity of gold nanorods: molecular origin of cytotoxicity and surface effects. Small 5(6):701–708. https://doi.org/10.1002/smll.200801546

Alkilany AM, Thompson LB, Boulos SP, Sisco PN, Murphy CJ (2012) Gold nanorods: their potential for photothermal therapeutics and drug delivery, tempered by the complexity of their biological interactions. Adv Drug Deliv Rev 64(2):190–199. https://doi.org/10.1016/j.addr.2011.03.005

An L, Yuanyuan Wang Y, Tian Q, Shiping Yang S (2017) Small gold nanorods: recent advances in synthesis, biological imaging, and cancer therapy. Materials (Basel) 10(12):1372. https://doi.org/10.3390/ma10121372

Bibikova O, Singh P, Popov A, Akchurin G, Skaptsov A, Skovorodkin I, Khanadeev V, Mikhalevich D, Kinnunen M, Akchurin G, Bogatyrev V, Khlebtsov N, Vainio SJ, Meglinski I, Tuchin V (2017) Shape-dependent interaction of gold nanoparticles with cultured cells at laser exposure. Laser Physics Letters 14(5):055901. https://doi.org/10.1088/1612-202X/aa63ae

Chateau D, Liotta A, Vadcard F, Navarro JRG, Chaput F, Lerme J, Lerouge F, Parola S (2015) From gold nanobipyramids to nanojavelins for a precise tuning of the plasmon resonance to the infrared wavelengths experimental and theoretical aspects. Nanoscale 7(5):1934–1943. https://doi.org/10.1039/c4nr06323f

Deng J, Yao M, Gao C (2017) Cytotoxicity of gold nanoparticles with different structures and surface-anchored chiral polymers. Acta Biomater 53:610–618. https://doi.org/10.1016/j.actbio.2017.01.082

Domey J, Teichgräber U, Hilger I (2015) Gold nanoparticles allow detection of early-stage edema in mice via computed tomography imaging. Int J Nanomedicine 10:3803–3814. https://doi.org/10.2147/IJN.S77383

Duan X, Li Y (2013) Physicochemical characteristics of nanoparticles affect circulation, biodistribution, cellular internalization, and trafficking. Small 9-10:1521–1532. https://doi.org/10.1002/smll.201201390

Evcimen NI, Coskun S, Kozanoglu D, Ertas G, Unalanbc HE, Esenturk EN (2015) Growth of branched gold nanoparticles on solid surfaces and their use as surface-enhanced Raman scattering substrates. RSC Adv 5:101656–101663. https://doi.org/10.1039/C5RA18570J

Fard JK, Jafari S, Eghbal MA (2015) A review of molecular mechanisms involved in toxicity of nanoparticles. Adv Pharm Bull 5(4):447–454. https://doi.org/10.15171/apb.2015.061

Favi PM, Gao M, Arango JS, Ospina SP, Morales M, Pavon JJ, Webster TJ (2015) Shape and surface effects on the cytotoxicity of nanoparticles: goldnanospheres versus gold nanostars. J Biomed Mater Res A 103(11):3449–3462. https://doi.org/10.1002/jbm.a.35491

Feng J, Chen L, Xia Y, Xing J, Li Z, Qian Q, Wang Y, Wu A, Zeng L, Zhou Y (2017) Bioconjugation of gold nanobipyramids for SERS detection and targeted photothermal therapy in breast cancer. ACS Biomater Sci Eng 3:608–618. https://doi.org/10.1021/acsbiomaterials.7b00021

Fratoddi I, Venditti I, Cametti C, Russo MV (2015) How toxic are gold nanoparticles? The state-of-the-art. Nano Res 8(6): 1771–1799. https://doi.org/10.1088/1612-202X/aa63ae

Guidance document on using in vitro data to estimate in vivo starting doses for acute toxicity 2001. National Institute of Environmental Health Sciences, National Institutes of Health, US Public Health Service, NIH Publication No. 01-4500 https://ntp.niehs.nih.gov/iccvam/docs/acutetox_docs/guidance0801/iv_guide.pdf. Accessed 30 Jan 2020

Jia YP, Ma BY, Wei XW, Qian ZY (2017) The in vitro and in vivo toxicity of gold nanoparticles. Chinese Chem Lett 28(4):691–702. https://doi.org/10.1016/j.cclet.2017.01.021

Kokkinopoulou M, Simon J, Landfester K, Mailänder V, Lieberwirth I (2017) Visualization of the protein corona: towards a biomolecular understanding of nanoparticle-cell-interactions. Nanoscale 9:8858–8870. https://doi.org/10.1039/C7NR02977B

Lee YJ, Ahn EY, Park Y (2019) Shape-dependent cytotoxicity and cellular uptake of gold nanoparticles synthesized using green tea extract. Nanoscale Res Lett 14(1):129. https://doi.org/10.1186/s11671-019-2967-1

Li Y, Monteiro-Riviere NA (2016) Mechanisms of cell uptake, inflammatory potential and protein corona effects with gold nanoparticles. Nanomed (Lond) 11(24):3185–3203. https://doi.org/10.2217/nnm-2016-0303

Maria João Oliveira MJ, de Almeida MP, Nunes D, Fortunato E, Martins R, Pereir E, Byrne HJ, Águas H, Franco R (2019) Design and simple assembly of gold nanostar bioconjugates for surface-enhanced Raman spectroscopy immunoassays. Nanomaterials 9:1561. https://doi.org/10.3390/nano9111561

McQuaid HN, Muir MF, Taggart LE, McMahon SJ, Coulter JA, Hyland WB, Jain S, Butterworth KT, Schettino G, Prise KM, Hirst DG, Botchway SW, Currell FJ (2016) Imaging and radiation effects of gold nanoparticles in tumour cells. Sci Rep 6:19442. https://doi.org/10.1038/srep19442

Navyatha B, Nara S (2019) Gold nanostructures as cancer theranostic probe: promises and hurdles. Nanomedicine 14(6):766–796. https://doi.org/10.2217/nnm-2018-0170

Nikoobakht B, El-Sayed MA (2003) Preparation and growth mechanism of gold nanorods (nrs) using seed-mediated growth method. Chem Mater 15(10):1957–1962. https://doi.org/10.1021/cm020732I

Quaresma P, Osorio I, Doria G, Carvalho PA, Pereira A, Langer J, Araujo JP, Pastoriza-Santos I, Liz-Marzan LM, Franco R, Baptistac PV, Pereira E (2014) Star-shaped magnetite@gold nanoparticles for protein magnetic separation and SERS detection. RSC Adv 4:3659–3667. https://doi.org/10.1039/C3RA46762G

Sasidharan S, Bahadur D, Srivastava R (2016) Albumin stabilized gold nanostars: a biocompatible nanoplatform for SERS, CT imaging and photothermal therapy of cancer. RSC Adv 6(87):84025–84034. https://doi.org/10.1039/C6RA11405A

Sharma A, Madhunapantula SRV, Robertson GP (2012) Toxicological considerations when creating nanoparticle based drugs and drug delivery systems. Expert Opin Drug Metab Toxicol 8(1):47–69. https://doi.org/10.1517/17425255.2012.637916

Silveira MC, Zumpano R, Moreira M, de Almeida MP, Oliveira MJ, Bento M, Montez C, Paixão I, Franco R, Pereira E, Almeida MG (2019) Star-shaped gold nanoparticles as friendly interfaces for protein electrochemistry: the case study of cytochrome c. Chem Electro Chem 6:4696–4703. https://doi.org/10.1002/celc.201901393

Steckiewicz KP, Barcinska E, Malankowska A, Zauszkiewicz-Pawlak A, Nowaczyk G, Zaleska-Medynska A, IInkielewicz-Stepniak I (2019) Impact of gold nanoparticles shape on their cytotoxicity against human osteoblast and osteosarcoma in in vitro model. Evaluation of the safety of use and anti-cancer potential. J Mater Sci Mater Med 30:22. https://doi.org/10.1007/s10856-019-6221-2

Stolle LB, Hussain S, Schlager JJ, Hofmann MC (2005) In vitro cytotoxicity of nanoparticles in mammalian germline stem

cells. Toxicol Sci 88(2):412–419. https://doi.org/10.1093/toxsci/kfi256

Tian Y, Luo S, Yan H, Teng Z, Pan Y, Zeng L, Wu J, Li Y, LiuY WS, Lu G (2015) Gold nanostars functionalized with amine-terminated PEG for X-ray/CT imaging and photothermal therapy. J Mater Chem B 3:4330–4337. https://doi.org/10.1039/C5TB00509D

Wang Y, Black KCL, Luehmann H, Li W, Zhang Y, Cai X, Wan D, Liu SY, Li M, Kim P, Li Z-Y, Wang LV, Liu Y, Xia Y (2013) Comparison study of gold nanohexapods, nanorods, and nanocages for photothermal cancer treatment. ACS Nano 7(3):2068–2077. https://doi.org/10.1021/nn304332s

Wang Z, Xie D, Liu H, Bao Z, Wang Y (2016) Toxicity assessment of precise engineered gold nanoparticles with different shapes in zebra fish embryos. RSC Adv 6(39):33009–33013. https://doi.org/10.1039/C6RA00632A

Wozniak A, Malankowska A, Nowaczyk G, Grzekowiak BF, Tunio K, Somski R, Medynska AZ, Jurga S (2017) Size and shape-dependent cytotoxicity profile of gold nanoparticles for biomedical applications. J Mater Sci Mater Med 28(6):92. https://doi.org/10.1007/s10856-017-5902-y

Xie X, Liao J, Shao X, Li Q, Lin Y (2017) The effect of shape on cellular uptake of gold nanoparticles in the forms of stars, rods, and triangles. Sci Rep 7:3827. https://doi.org/10.1038/s41598-017-04229-z

Yuan H, Khoury CG, Hwang H, Wilson CM, Grant GA, Vo-Dinh T (2012) Gold nanostars: surfactant-free synthesis, 3d modelling, and two-photon photoluminescence imaging. Nanotechnology 23(7):075102. https://doi.org/10.1088/0957-4484/23/7/075102

Zhang Z, Lin M (2014) Fast loading of PEG-SH on CTAB-protected gold nanorods. RSC Adv 4(34):17760–17767. https://doi.org/10.1039/C3RA48061E

Zhang XD, Wu HY, Wu D, Wang YY, Chang JH, Zhai ZB, Meng AM, Liu PX, Zhang LA, Fan FY (2010) Toxicologic effects of gold nanoparticles in vivo by different administration routes. Int J Nanomedicine 5:771–778. https://doi.org/10.2147/IJN.S8428

Zhao S, Tian Y, Liu W, Su Y, Zhang Y, Teng Z, Zhao Y, Wang S, Lu G, Yu Z (2018) High and low molecular weight hyaluronic acid-coated gold nanobipyramids for photothermal therapy. RSC Adv 8(16):9023–9030. https://doi.org/10.1039/C7RA11667E